(Received 18 October 2025, Accepted 13 November 2025, Scheduled 19 November 2025)

A Miniaturized 5G Microstrip Patch Antenna Element and MIMO Design

Xiao-Mei Ni[1] and Xin-Hao Ding[2,*]

[1] School of Aeronautic Engineering, Nanjing University of Industry Technology, Nanjing 210023, China
[2] School of Information Science and Technology, Nantong University, Nantong 226019, China

ABSTRACT: This paper proposes a novel microstrip patch antenna element and MIMO design based on quarter-mode substrate integrated waveguide (QMSIW). This design not only achieves antenna miniaturization but also effectively reduces the mutual coupling between antenna elements. The antenna element employs a triangular patch as the main radiator, with its long side grounded via two metal cavities. For bandwidth enhancement, a T-shaped strip is positioned at the center of the triangular patch's long side, and a new mode is introduced. A pair of slots is etched at the junction between the strip and the patch; adjusting the slot size enables dual-mode operation and control coupling. Building on this element, a 2×2 MIMO system is developed, featuring a compact size and requiring only one dielectric substrate, thereby achieving high integration and low cost. The patch occupies an area of $(0.22 \times 0.22\lambda_0^2)/2$, while the strip occupies $0.066 \times 0.068\lambda_0^2$ with high integration. The antenna achieves N78 band coverage with a total area of $0.0287\lambda_0^2$. Experimental results demonstrate an 8.9% -10 dB impedance bandwidth (3.30–3.61 GHz) and -16 dB isolation, ensuring excellent overall performance. The antenna offers an effective solution for future 5G wireless communication systems.

1. INTRODUCTION

In the field of wireless communications, microstrip patch antennas (MPAs) have been widely used due to their low cost and light weight [1, 2]. Various types of microstrip antennas have been proposed in the past. In [3, 4], parasitic patches are placed above the main radiating patch to realize stacked antennas. In [5, 6], an antenna operates in a metasurface manner, where the higher-order modes of the metasurface can be controlled to enhance bandwidth. In [7, 8], the patch mode and feed slot mode work collaboratively. In [9, 10], an antenna adopts multi-resonator technology. However, the above MPAs are only limited to the study of antenna elements and have not been studied for multiple-input multiple-output (MIMO) technology. MIMO can significantly increase the channel capacity of wireless communication systems without requiring additional spectrum or power resources [11–13], and is widely used in modern wireless communication systems.

However, to implement MIMO, the close arrangement of antenna elements in compact terminals or portable devices will lead to high mutual coupling, which degrades the performance of spatial diversity and multiplexing [14, 15]. Therefore, a large number of decoupling methods have been proposed. In [16–18], defected ground structures (DGSs) act as spatial band-stop filters by etching half-wavelength resonant slots on the ground plane to reduce coupling between antennas. In [19], short-circuit pins are introduced in stacked microstrip patch antenna arrays to generate coupling zeros. By forming currents with approximately equal amplitudes but opposite phases on different regions of the patch, electric field components are canceled out to achieve high isolation. In [20], an inductance-based decoupling scheme is proposed, using a combined mode cancellation method of common-mode and differential-mode to reduce the mutual coupling between MPAs with extremely close spacing. Inserting lumped inductors between the ground planes of the elements can effectively suppress the original strong coupling. Although these types of antennas can achieve good decoupling effects, their antennas are still traditional MPAs, which still limit the further reduction of MIMO system size.

Antenna element miniaturization is not only conducive to the miniaturization of MIMO but also indirectly increases the boundary spacing between elements in the array, thereby improving the isolation between elements [21]. Compared with traditional MPAs [22] or planar inverted-F antennas (PIFAs) [23, 24], quarter mode substrate integrated waveguide (QMSIW) antennas usually have more compact dimension [25]. Therefore, if QMSIW can be applied to MIMO design, miniaturization can be effectively achieved.

In this paper, a novel antenna element is first designed based on QMSIW. The main radiator of the antenna element is a triangular metal patch, and the long side of the patch is grounded through two metallized cavities to operate in the quarter-mode. To introduce a new resonant mode for bandwidth enhancement, a T-shaped metal strip is placed at the center of the long side of the triangular metal patch and connected to the metal patch. Subsequently, a slot is etched at the connection between the T-shaped metal strip and triangular metal patch. By adjusting the size of the slot, the T-shaped strip mode can be shifted to merge with the patch mode, achieving dual-mode operation. Subsequently, a 2×2 MIMO system is designed based on the antenna element. This design, due to operating in the quarter-mode,

* Corresponding author: Xin-Hao Ding (xhding1@hotmail.com).

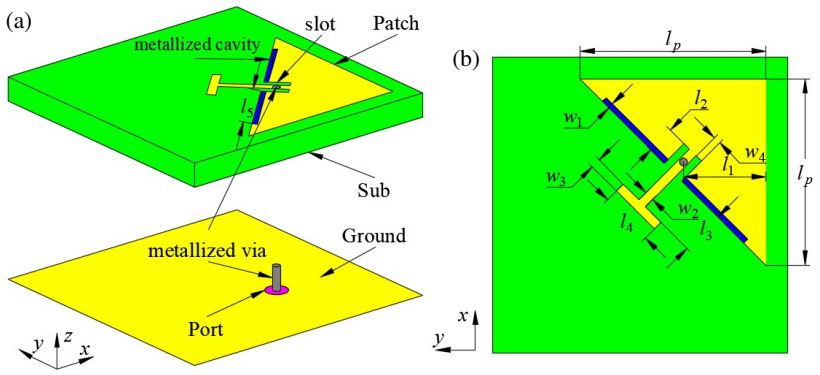

FIGURE 1. Configuration of the antenna element. (a) 3D view, (b) Side view.

achieves a compact size and uses only a single-layer dielectric substrate. The main innovation points include:

1) By combining triangular patches with T-shaped metal strips, dual-mode operation is achieved to expand the bandwidth.

2) The resonant mode is adjusted by slotting to effectively control the coupling.

3) The antenna element is small in size $(0.22 \times 0.22\lambda_0^2)/2$, with a compact overall structure and high integration.

4) The isolation degree of -16 dB has been achieved in the MIMO system, with good performance.

2. ANTENNA STRUCTURE AND DESIGN

2.1. Antenna Structure

Figure 1 shows the structure of the miniaturized antenna, which includes a triangular metal patch, a dielectric substrate, and a metal ground. The antenna is constructed based on only one layer of dielectric substrate, with FR4 used as the substrate material, having a dielectric constant (ε_r) of 4.4 and a loss tangent ($\tan\delta$) of 2×10^{-2}. The triangular metal patch and metal ground are printed on the upper and lower surfaces of the substrate, respectively. In addition, two metallized cavities are formed on the substrate and connected to the long side portion of the triangular patch, allowing the triangular metal patch to resonate in a quarter-mode. A T-shaped metal strip is connected to the patch at the center of the long side of the patch, and two pairs of slots are etched on the patch. The feeding position is set on a line at a 45° direction along the x-axis, and the antenna is excited using coaxial feeding, where the inner conductor of the coaxial cable is connected to a metallized via and the outer conductor connected to the metal ground. Table 1 gives the detailed dimensional parameters of the antenna.

2.2. Element Design

Figure 2 shows the design process of the antenna element, which can be divided into four steps. Model 1, as shown in Figure 2(a), consists of a square resonator surrounded by four rows of metallized cavities. It can resonate as a complete cavity

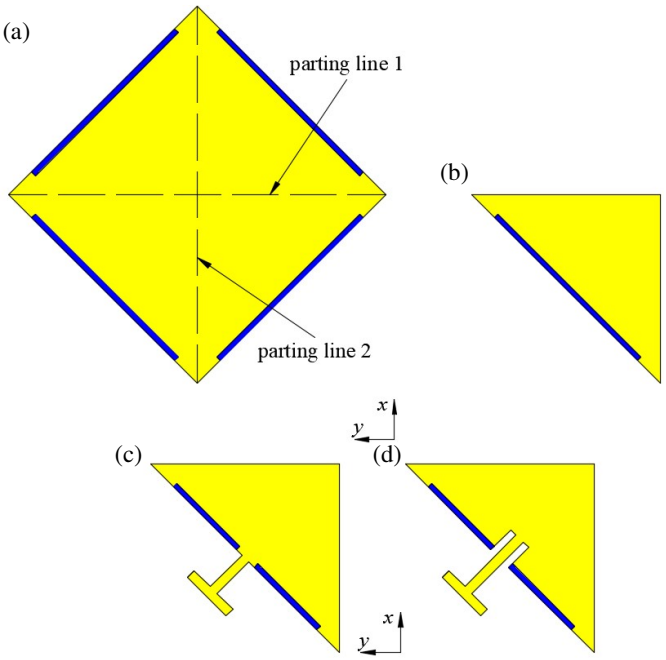

FIGURE 2. Antenna element design process. (a) Mode 1, (b) Mode 2, (c) Mode 3, (d) Mode 4.

TABLE 1. Parameters of the antenna (mm).

Parameter	Value	Parameter	Value
l_p	19.56	w_1	0.52
l_1	8.7	w_2	1.01
l_2	2.91	w_3	1
l_3	4.63	w_4	0.8
l_4	5.68	r	0.4
l_5	9.19	H	2.8

antenna in the TE_010 fundamental mode, which can be called full mode. Obviously, Model 1 occupies a large size, which is inconsistent with the miniaturization design concept of the terminal antenna, so size reduction is needed. Model 2, as shown in Figure 2(b), is achieved by dividing the cavity that realizes the full-mode resonance along division lines 1 and 2 along the y-axis and x-axis based on Model 1. By introducing virtual

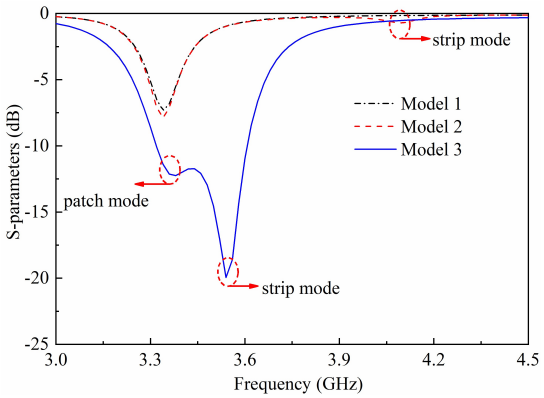

FIGURE 3. S-parameters corresponding to model 2, Model 3 and Model 4.

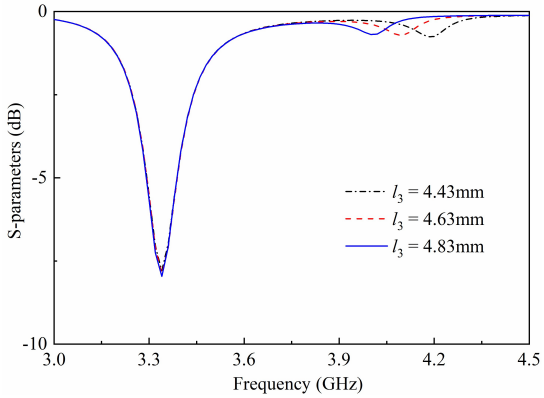

FIGURE 4. The influence of l_3 on the S-parameter of Model 3.

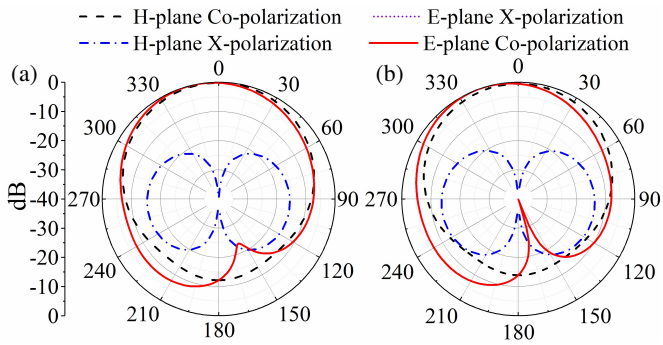

FIGURE 5. The radiation patterns of the antenna at 3.35 GHz. (a) Mode 3, (b) Mode 4.

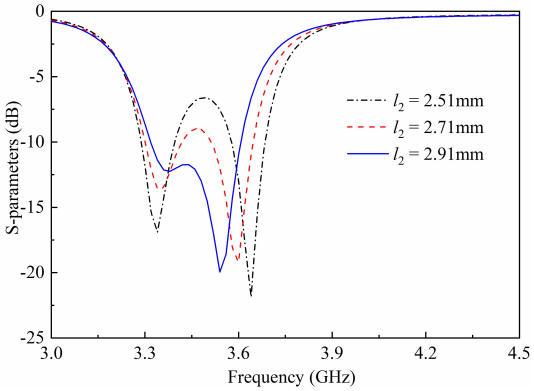

FIGURE 6. The influence of l_2 on the S-parameter of Model 4.

magnetic walls, three-quarters of the structure can be removed, thereby effectively reducing the total size of the antenna element. Model 2 resonates in the quarter-mode, as shown in Figure 3, with its resonant mode located at 3.35 GHz. However, although the size is reduced, due to having only one mode, it will result in a narrow bandwidth.

To broaden the bandwidth, a T-shaped metal strip is introduced at the center of the long side of the triangular metal patch, specifically in the blank area between the two metal slots, and connected to the metal patch, as shown in Figure 2(c). As shown in Figure 3, the T-shaped metal strip can introduce a new mode at 4 GHz, and the position of strip mode can be adjusted by changing geometric parameters of the strip. Figure 4 verifies the mode of the strip: as the size of the strip increases, its mode frequency shifts to lower frequencies, fully proving that the new mode is introduced by the strip. Figure 5 shows the radiation performance of the triangular patch before and after loading the T-shaped strip. It can be seen that there is almost no change in the radiation pattern of the patch at its resonant point before and after loading, thus proving that the loading of the strip has almost no effect on the radiation performance of the triangular patch.

Subsequently, in order to reduce the frequency of the strip mode without increasing the size, slots are etched in the portion where the T-shaped strip is connected to the triangular metal patch, as shown in Figure 2(d). The position of the strip mode can be controlled by precisely adjusting the geometric parameters of the slots, reducing the frequency of the strip mode from 4 GHz to 3.55 GHz, as shown in Figure 3. Finally, the patch mode and strip mode can be combined to form dual-mode operation, enhancing the bandwidth.

To verify the rationality of this design, a parametric study was conducted on Model 4. Figure 6 shows the effect of slot length (l_2) on the S-parameters. As l_2 increases, the high-frequency mode shifts upward, while the low-frequency mode remains basically unchanged, indicating that it is feasible to control the low-frequency mode through the slot. Figure 7 shows the simulated electric field distribution of the antenna at 3.35 GHz and 3.55 GHz. At 3.35 GHz, the strong electric field on the trian-

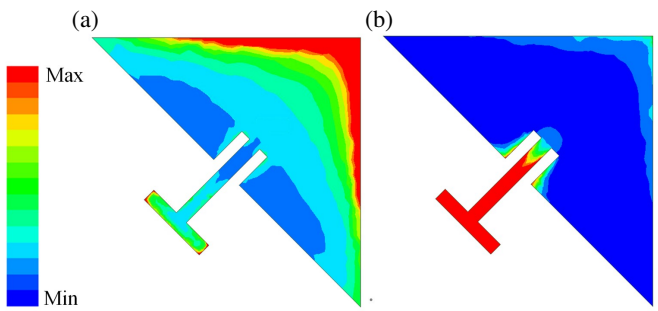

FIGURE 7. Antenna mode electric field distribution. (a) 3.35 GHz, (b) 3.55 GHz.

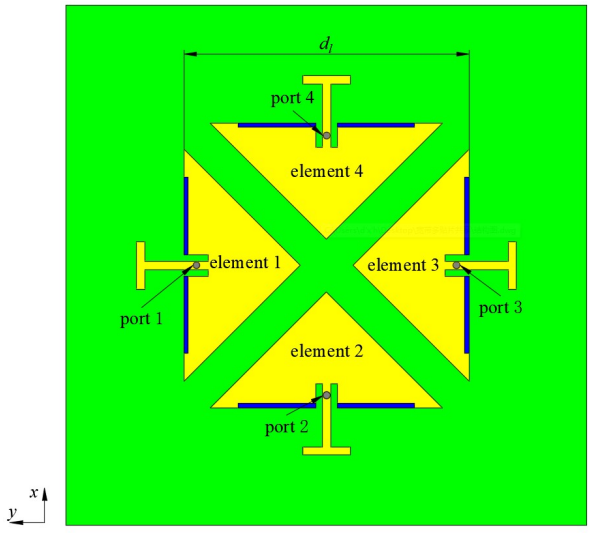

FIGURE 8. Configuration of the MIMO.

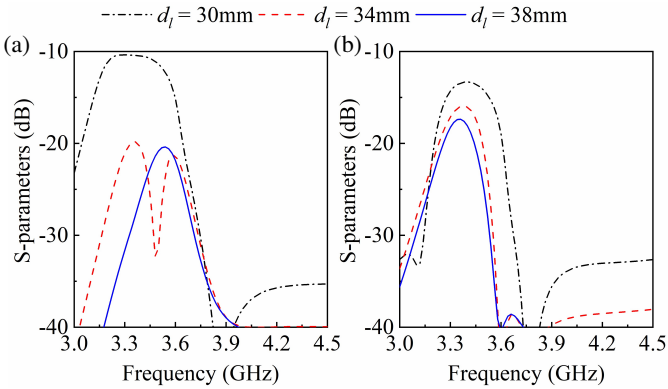

FIGURE 9. The influence of d_l on the isolation of MIMO. (a) Port 1 and Port 2, (b) Port 1 and Port 3.

gular patch and weak electric field at the strip indicate that this mode is mainly caused by the triangular patch, dominated by the quarter-mode. At 3.55 GHz, the strong electric field in the T-shaped strip indicates that the working mode at this time is dominated by the strip mode.

2.3. MIMO Design

The above antenna element can be expanded into a 4×4 MIMO configuration, as shown in Figure 8. Ports 1, 2, 3, and 4 can be fed individually, corresponding to Element 1, Element 2, Element 3, and Element 4, respectively. As shown in Figure 9, the effect of dimension d_l on isolation is studied. As d_l decreases, the isolation between antenna elements becomes smaller. Finally, $d_l = 15$ mm is selected to ensure 16 dB isolation under the minimum size of the MIMO antenna.

The surface currents of the patch are utilized to explain the coupling/decoupling mechanism. Two distinct spacing conditions ($d_l = 30$ mm and $d_l = 34$ mm) are compared, as shown in Figure 10. When Element 1 is excited, it is observed that when d_l is 34 mm, the coupling current of Element 2 is significantly smaller than when d_l is 30 mm. Therefore, it can be demonstrated that as d_l increases, the decoupling effect improves progressively.

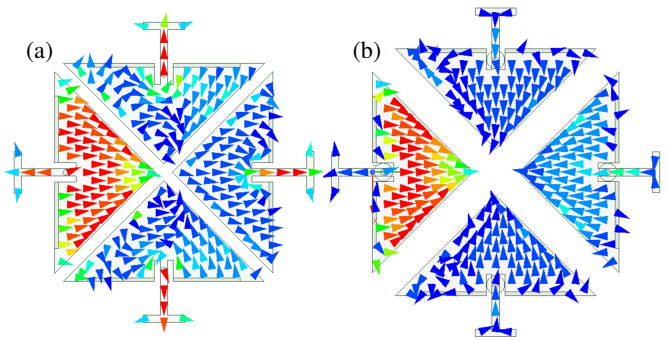

FIGURE 10. The surface currents of the patch in two distinct spacing conditions (a) $d_l = 30$ mm, (b) $d_l = 34$ mm.

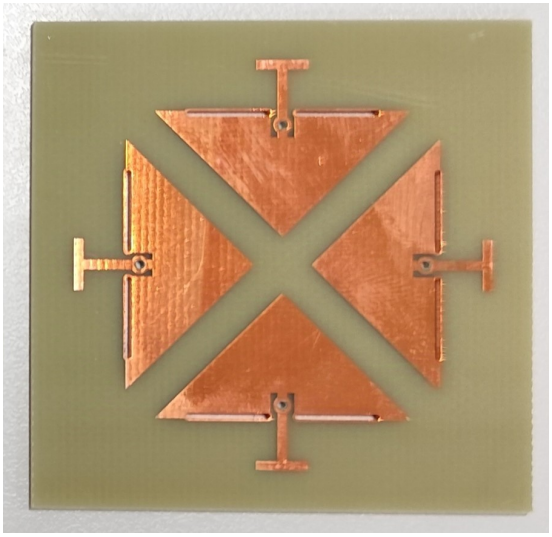

FIGURE 11. Picture of antenna prototype.

3. SIMULATION AND MEASURED RESULTS

To verify the design, the MIMO antenna is fabricated and tested, with Figure 11 showing the antenna prototype. Figure 12 presents the simulation and test results of the antenna's reflection coefficient and total efficiency. The measured -10 dB impedance bandwidth is 8.9% (from 3.30 GHz to 3.61 GHz), while the simulated bandwidth range is from 3.29 GHz to 3.60 GHz. Within the operating frequency band, the total efficiency of the antenna elements ranges from 45% to 55%, and the efficiencies from simulation and testing show good consistency. Figure 13 indicates that the isolation between elements remains over 16 dB. Figure 14 indicates that the elements achieve the envelope correlation coefficient (ECC) below 0.5, and the diversity gains (DGs) ranging from 8.5 dB to 10.1 dB. In Figure 15, the simulated and measured radiation patterns of Element 1 at 3.35 GHz and 3.55 GHz in the E- and H-planes show good consistency.

Table 2 shows the performance comparison between the antenna designed in this paper and several other antennas of the

TABLE 2. Performance comparisons with reported works.

Ref.	Frequency (GHz)	Element spacing (λ_0)	Element size (λ_0^2)	Profile (λ_0)	Bandwidth	Isolation (dB)
[17]	2.45	0.34	0.0529 (0.23 × 0.23)	0.012	2.0%	30
[18]	10	0.28	0.0625 (0.25 × 0.25)	0.1	22.2%	20
[19]	3.5	0.5	0.09 (0.30 × 0.30)	0.07	16.3%	43
[20]	2.45	0.44	0.2209 (0.47 × 0.47)	0.049	5.5%	15.4
This work	**3.5**	**0.23**	**0.0287 (0.22 × 0.22/2 + 0.066 × 0.068)**	**0.032**	**8.9%**	**16**

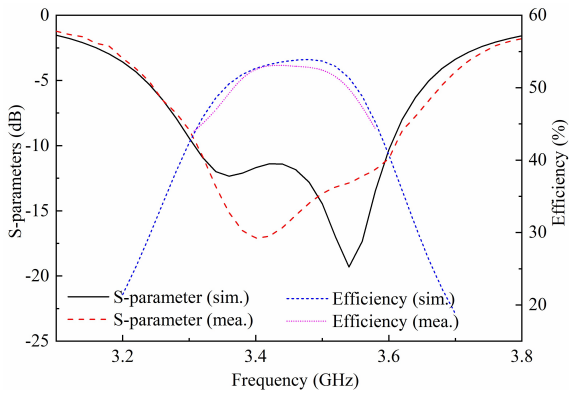

FIGURE 12. Simulated and measured results of antenna reflection coefficient and total efficiency.

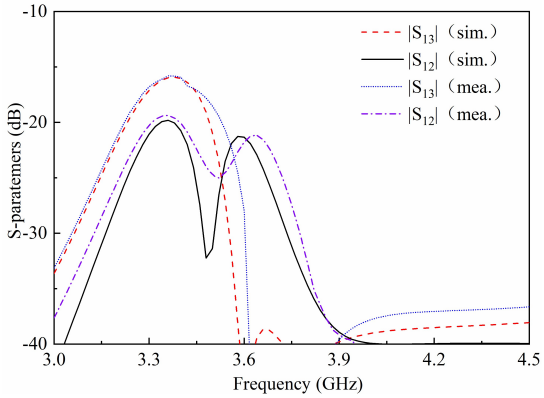

FIGURE 13. Simulated and measured isolations between elements.

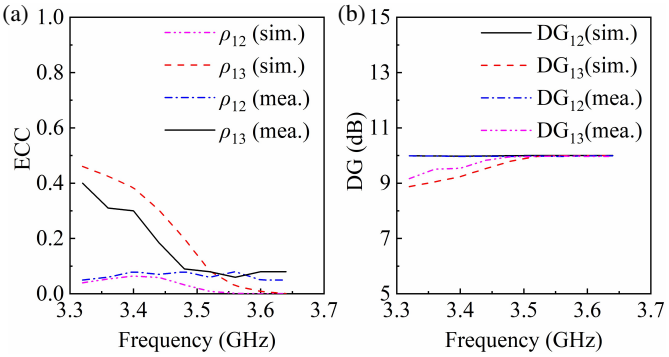

FIGURE 14. Simulated and measured (a) ECC and (b) DG of the MIMO antenna.

same type. It can be seen that due to the use of a quarter-mode operation, this design has the smallest planar size and the smallest element spacing.

4. CONCLUSION

In this paper, a miniaturized antenna element based on QMSIW is proposed. It adopts a triangular metal patch design and achieves dual-mode operation with bandwidth widened by introducing T-shaped metal strips and slots. Based on this, a 2×2 MIMO system is designed and fabricated for testing. This design has the advantages of compact size, high integration, and low cost, providing a new direction for future research and applications of 5G terminal antennas.

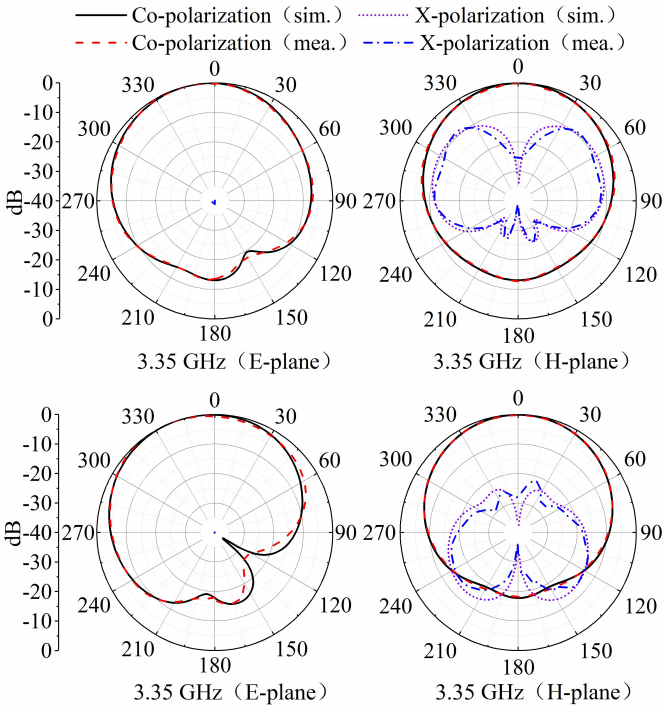

FIGURE 15. Simulated and measured radiation patterns of Element 1.

ACKNOWLEDGEMENT

This work was supported by the Talent Introduction Project of Nanjing University of Industry Technology under Grant YK23-03-05 and Nantong University under Grant 135424630060.

REFERENCES

[1] Xu, J., W. Hong, Z. H. Jiang, H. Zhang, and K. Wu, "Low-profile wideband vertically folded slotted circular patch array for Ka-band applications," *IEEE Transactions on Antennas and Propagation*, Vol. 68, No. 9, 6844–6849, 2020.

[2] Sun, L., Y. Li, and Z. Zhang, "Wideband decoupling of integrated slot antenna pairs for 5G smartphones," *IEEE Transactions on Antennas and Propagation*, Vol. 69, No. 4, 2386–2391, 2021.

[3] Tian, M., N. Yan, Y. Luo, and K. Ma, "A low-cost high-gain filtering patch antenna using SISL technology for 5G application," *IEEE Antennas and Wireless Propagation Letters*, Vol. 20, No. 12, 2270–2274, 2021.

[4] Ramírez, G. A., I. Zhou, S. Blanch, M. A. Towfiq, B. A. Cetiner, J. Romeu, and L. Jofre-Roca, "Reconfigurable dual-polarized beam-steering broadband antenna using a crossed-strips geometry," *IEEE Antennas and Wireless Propagation Letters*, Vol. 20, No. 8, 1379–1383, 2021.

[5] Liu, S., D. Yang, Y. Chen, X. Zhang, and Y. Xiang, "High isolation and low cross-polarization of low-profile dual-polarized antennas via metasurface mode optimization," *IEEE Transactions on Antennas and Propagation*, Vol. 69, No. 5, 2999–3004, 2021.

[6] De Dieu Ntawangaheza, J., L. Sun, Y. Li, D. Biao, Z. Xie, and G. Rushingabigwi, "A single-layer planar low-profile wideband microstrip line-fed metasurface antenna," *IEEE Antennas and Wireless Propagation Letters*, Vol. 20, No. 9, 1641–1645, 2021.

[7] Zhang, X., T.-Y. Tan, Q.-S. Wu, L. Zhu, S. Zhong, and T. Yuan, "Pin-loaded patch antenna fed with a dual-mode SIW resonator for bandwidth enhancement and stable high gain," *IEEE Antennas and Wireless Propagation Letters*, Vol. 20, No. 2, 279–283, 2021.

[8] Liu, Q., L. Zhu, J. Wang, and W. Wu, "A wideband patch and SIW cavity hybrid antenna with filtering response," *IEEE Antennas and Wireless Propagation Letters*, Vol. 19, No. 5, 836–840, 2020.

[9] Wang, J., Y. Li, and J. Wang, "A low-profile dual-mode slot-patch antenna for 5G millimeter-wave applications," *IEEE Antennas and Wireless Propagation Letters*, Vol. 21, No. 3, 625–629, 2022.

[10] Gan, Z. and Z.-H. Tu, "Dual-mode conjoint patch-pair for 5G wideband patch antenna array application," *IEEE Antennas and Wireless Propagation Letters*, Vol. 20, No. 2, 244–248, 2021.

[11] Yin, Y., B. Ustundag, K. Kibaroglu, M. Sayginer, and G. M. Rebeiz, "Wideband 23.5–29.5-GHz phased arrays for multistandard 5G applications and carrier aggregation," *IEEE Transactions on Microwave Theory and Techniques*, Vol. 69, No. 1, 235–247, 2021.

[12] Wang, S., A. Alhamed, and G. M. Rebeiz, "An 8-element 5G multistandard 28-/39-GHz dual-band, dual-polarized phased array for compact systems," *IEEE Transactions on Microwave Theory and Techniques*, Vol. 71, No. 9, 4109–4118, 2023.

[13] Li, Y., H. Zou, M. Wang, and G. Yang, "Design of a wideband 8-element MIMO antenna for 5G communication," *Chinese Journal of Radio Science*, Vol. 33, No. 4, 447–454, 2020.

[14] Jensen, M. A. and J. W. Wallace, "A review of antennas and propagation for MIMO wireless communications," *IEEE Transactions on Antennas and Propagation*, Vol. 52, No. 11, 2810–2824, 2004.

[15] Wang, B., Y. Chang, and Y. Sun, "Performance of the large-scale adaptive array antennas in the presence of mutual coupling," *IEEE Transactions on Antennas and Propagation*, Vol. 64, No. 6, 2236–2245, 2016.

[16] Gao, D., Z.-X. Cao, S.-D. Fu, X. Quan, and P. Chen, "A novel slot-array defected ground structure for decoupling microstrip antenna array," *IEEE Transactions on Antennas and Propagation*, Vol. 68, No. 10, 7027–7038, 2020.

[17] Qian, B., X. Huang, X. Chen, M. Abdullah, L. Zhao, and A. A. Kishk, "Surrogate-assisted defected ground structure design for reducing mutual coupling in 2 × 2 microstrip antenna array," *IEEE Antennas and Wireless Propagation Letters*, Vol. 21, No. 2, 351–355, 2022.

[18] Ma, L., Z. Shao, J. Lai, C. Gu, and J. Mao, "A compact dual-decoupling scheme for aperture-coupled and probe-fed closely spaced wideband microstrip antennas," *IEEE Transactions on Antennas and Propagation*, Vol. 71, No. 11, 9072–9077, 2023.

[19] Fang, Y., L.-S. Wu, L.-F. Qiu, and Y. P. Zhang, "A method of introducing coupling null by shorting pins for stacked microstrip patch antenna array," *IEEE Transactions on Antennas and Propagation*, Vol. 70, No. 7, 6030–6035, 2022.

[20] Sun, L., Y. Li, and Z. Zhang, "Decoupling between extremely closely spaced patch antennas by mode cancellation method," *IEEE Transactions on Antennas and Propagation*, Vol. 69, No. 6, 3074–3083, 2021.

[21] Ding, X.-H., J.-Y. Yang, W.-W. Yang, and J.-X. Chen, "Compact dual-band and dual-polarized base station antenna with shared-dipole elements," *IEEE Antennas and Wireless Propagation Letters*, Vol. 22, No. 6, 1371–1375, 2023.

[22] Dai, Y., W. Li, S. Jiang, P.-C. Wang, and Z.-B. Wang, "Broadband and low-profile patch antenna based on multimode resonance," *Chinese Journal of Radio Science*, Vol. 37, No. 4, 670–677, 2022.

[23] Liu, N.-W., L. Zhu, Z.-X. Liu, Z.-Y. Zhang, G. Fu, and Y. Liu, "Cross-polarization reduction of a shorted patch antenna with broadside radiation using a pair of open-ended stubs," *IEEE Transactions on Antennas and Propagation*, Vol. 68, No. 1, 13–20, 2020.

[24] Wang, Y.-X., "Research on key technologies of low-profile wideband antenna array," Ph.D. dissertation, University of Electronic Science and Technology of China, Chengdu, China, 2024.

[25] Yang, T., Z. Zhao, D. Yang, and Z. Nie, "A single-layer circularly polarized antenna with improved gain based on quarter-mode substrate integrated waveguide cavities array," *IEEE Antennas and Wireless Propagation Letters*, Vol. 19, No. 12, 2388–2392, 2020.